The Bering Slope Current System Revisited*

GREGORY C. JOHNSON AND PHYLLIS J. STABENO

NOAA/Pacific Marine Environmental Laboratory, Seattle, Washington

STEPHEN C. RISER

School of Oceanography, University of Washington, Seattle, Washington

Journal of Physical Oceanography

Submitted 13 January 2003

---

* PMEL Contribution Number 2540

Corresponding author address: Dr. Gregory C. Johnson, NOAA/Pacific Marine Environmental Laboratory, 7600 Sand Point Way N.E., Bldg. 3, Seattle, WA 98115-6349. E-mail: gjohnson@pmel.noaa.gov.

ABSTRACT

Mean circulation and water properties within the Aleutian Basin of the Bering Sea are investigated using hydrographic and Lagrangian displacement data from an array of 14 profiling CTD floats in the region. The floats cycle between a park pressure of 1000 dbar and the surface. After 10 days at park pressure they rise to the surface, measure temperature and salinity profiles, and then transmit these data via satellite before sinking again. The only coherent mean velocity pattern measured at 1000-dbar is a northwestward flow of a few cm s^{-1} along the northeastern boundary of the basin, the deep signature of the Bering Slope Current. Water property distributions around the shallow temperature minimum and the deeper temperature maximum are consistent with advection of warm water from the south moving cyclonically around the basin, eastward in the Aleutian North Slope Current and then northwestward in the Bering Slope Current. The geostrophic transport field between the surface and the park pressure relative to that pressure also shows cyclonic motion, although there is significant noise, likely owing to the influence of mesoscale eddies. The mean along-slope geostrophic transport of the Bering Slope Current is determined between 0 and 1600 dbar relative to the park pressure and then combined with mean along-slope velocities at the park pressure to estimate an absolute transport of the current offshore of the 1000-m isobath and between 0 to 1600 dbar of 4.2 (±1.1) × 10^6 m^3 s^{-1}, where the uncertainties are 95% confidence intervals.

1. Introduction

The Bering Sea, located between Siberia and Alaska, is bounded to the south by the arc of the Komandorskiye and Aleutian Islands and to the north by Siberia, with a narrow connection to the Arctic Ocean through the Bering Strait (Fig. 1). The northeast portion of the sea is a wide and shallow continental shelf. The deep portion of the sea is divided into three connected deep basins, the largest of which is the Aleutian Basin. The smaller Bowers Basin is partly enclosed by the Bowers Ridge, and the equally small Kamchatka Basin is partly enclosed by the Shirshov Ridge. While the Bering Strait to the north is shallow, there are numerous passes and straits within the island arc to the south, with the deepest three being Kamchatka Strait (164° E, ~3600-m sill depth), Near Strait (170° E, ~2000 m), and Amchitka Strait (180°, ~1000 m).

The surface circulation of the Bering Sea has been estimated using satellite-tracked drifters (Stabeno and Reed 1994), and can very roughly be described as a cyclonic gyre (Stabeno et al. 1999). Currents within the region include an eastward flow along the southern boundary of the deep Bering Sea, fed by northward flow through the island arc passes and straits mentioned above (Reed and Stabeno 1994), named the Aleutian North Slope Current; a northwestward flow along the northeast continental slope of the Aleutian Basin, the Bering Slope Current (Kinder et al. 1975); and a southward flow offshore of Kamchatka that exits the Bering sea through the Kamchatka Strait, the Kamchatka Current (Verkhunov and Tkachenko 1992). However, apart from a few isolated current meter records (Schumacher and Reed 1992, Cokelet and Stabeno 1997), there are very few direct measurements of the subsurface flow in the deep Bering Sea.

Much of the knowledge of the subsurface circulation of the Bering Sea has come through application of the geostrophic relation to data from hydrographic surveys to estimate the flow field relative to a reference level of no motion, or occasionally, one of known motion. In the Bering Sea, a level of no motion is often assumed to hold somewhere between 500 m and 1500 m (Kinder et al. 1975, Reed 1995). This assumption is often necessitated by hydrographic station data that stop at mid-depth. The assumption is also usually applied with the acknowledgement that the level of no motion is in reality likely to be a level of weak motion. Since the absolute velocity field is only known in a few isolated locations at depth (and the surface velocity field measured by Lagrangian drifters is not expected to be in close geostrophic balance because of near-surface Ekman dynamics), often no better alternative has been available. Water property distributions from hydrographic surveys, such as the relative strength of the subsurface temperature minimum (Kinder et al. 1975), are sometimes used to corroborate geostrophic calculations.

Despite the prevalence of mid-depth levels of no motion in the Bering Sea literature, the few full-depth hydrographic surveys there (Roden 1995) show that geostrophic shear, while it weakens with increasing depth, can extend to the abyssal sea floor. In fact, referencing geostrophic velocities to a level of known motion using velocity data from a shipboard acoustic Doppler current profiler (ADCP) has shown that velocities extend much deeper than 500 to 1500 m in the Bering Sea, with geostrophic values of a few cm s^{-1} even at the abyssal sea floor (Cokelet et al. 1996). While application of a mid-depth level of no motion apparently does not introduce a strong error in near-surface velocity estimates within the boundary currents (Reed 1995), it can introduce 1^{st} order error in the boundary current transport estimates, because even weak deep velocities result in large transports when

integrated over current cross-sections (Cokelet et al. 1996).

Other potentially confounding influences on current transport estimates are the energetic eddies that are so prevalent in the Bering Sea (Kinder et al. 1980, Schumacher and Stabeno 1994, Okkonen 2001, Mizobata et al. 2002). Most synoptic hydrographic surveys contain such eddies, whether they resolve them or not, and eddies at the edge of a hydrographic survey that are not sampled completely can badly bias transport estimates. Combining velocity data from drifters (Kinder et al 1980) and shipboard ADCPs (Cokelet et al. 1996) with hydrographic data suggests these eddies have a significant expression (several cm s^{-1}) at mid-depth, and even at the abyssal sea floor.

Finally, there is a strong seasonal cycle in wind forcing over the deep Bering Sea (Bond et al. 1994), with Ekman suction sufficient to drive a cyclonic gyre in topographic Sverdrup balance in the Bering Sea with a volume transport as large as 15 Sv (1 Sv = 1×10^6 m^3 s^{-1}) in winter and as small as zero in the summer. Numerical model results suggest a strong seasonal variation in gyre strength (Overland et al. 1994). A spring hydrographic survey of the Kamchatka Current certainly showed a stronger transport than observed 6 months later in fall (Verkhunov and Tkachenko 1992). This change is consistent with this hypothesized seasonal cycle, but there are probably not enough hydrographic data to distinguish seasonal from interannual transport variations (Stabeno and Reed 1992).

Here we use hydrographic and Lagrangian displacement data from an array of 14 profiling floats deployed in the Aleutian Basin to investigate the water properties and absolute circulation there. The focus is on the southeast corner of the basin, including the Bering Slope Current. Float displacements at 1000-dbar are used to make estimates of the flow field at that pressure (Davis 1998). Vertical profiles of temperature and salinity from the floats are

used in geostrophic calculations which are then combined with the direct estimates of 1000-dbar velocity to determine an absolute flow field. The data are distributed over seasons and the mesoscale eddy field, so the errors from these sources of noise in the determination of a mean circulation can be estimated.

2. Data

Starting in May 2001, we deployed profiling CTD (Conductivity-Temperature-Depth) profiling floats in the Bering Sea Basin. The floats were built at the University of Washington from components purchased from Webb Research Corp. Each float was equipped with a SBE-41 CTD from SeaBird Electronics Inc. The floats are programmed to drift freely at a park pressure of 1000 dbar for ten days, then rise to the surface in under 3.5 hours, collecting CTD data at 60 predetermined pressures during their ascent. They then remain on the ocean surface for slightly less than 11 hours, where they transmit data and their positions are determined by satellite (Service ARGOS, Inc.). Every 4^{th} cycle the floats sink to 2000 dbar just before rising to the surface, collecting data at 70 pressures and remaining on the surface for less than 7 hours. The floats are designed to last about 140 cycles each, for a lifetime of 4 years. Over 19 months, 553 profiles from 14 floats have been collected in the Bering Sea.

The salinity measurements from the floats are remarkably stable with respect to the deep potential temperature-salinity (θ-S) relation. For instance, at $\theta = 2^{\circ}$C, the floats measure a mean and standard deviation S = 34.526 (±0.005). For comparison, values for the stations from the World Ocean Circulation Experiment (WOCE) section P14N taken across the

Aleutian Basin (59°N, 176°W to 51.5°N, 180°) in 1993 (Roden 1995) are S = 34.531 (±0.002). Thus the mean float S is only about 0.005 higher than that from WOCE, with a variability that, while 2.5 times that of WOCE, seems quite small for CTDs that have been in the field for up to 19 months. However, such stable S measurements appear typical of these instruments over even longer deployments. In light of this relative sensor stability, no attempt has been made to adjust these data with respect to the climatological θ-S relation (Wong et al. 2003).

The drift velocity at the park pressure is estimated from the difference in position and time between the last position fix before a float sinks and the first position fix after it rises again about 10 days later. Two possible sources of error arise from this simple method. The first error source is unmeasured surface drift, and the second influences of subsurface currents as the floats rise and sink. The mean and standard deviation of float drift speeds at the surface, 0.22 (±0.14) m s^{-1}, are much greater than those at park pressure, 0.039 (±0.025) m s^{-1}. The float stays on the surface for roughly 10 hours, and during that time a variable number of position fixes, 6 (±2), are obtained. Hence on average about 1/6 (or 1.6 hours) of the float surface drift is unmeasured and erroneously ascribed to the park velocities, introducing an error of roughly 4% in them. The ascent and descent rate of the floats, the mean stratification, and the surface and park drift speeds can be all be combined to estimate that subsurface currents introduce an additional error of roughly 6% in the park velocities. Since these two errors are likely to be somewhat correlated, they can be summed for a worst-case estimate of 10% error in the park velocities. To date 554 park displacements have been measured in the Bering Sea, over 15 float-years worth of data.

These floats do occasionally run aground, potentially introducing significant biases into

their displacement data. If either the last position fix before descent or the first position fix after surfacing is over water shallower than 1000 m, according to a high resolution bathymetry (Smith and Sandwell 1997, version 8.2), the park depth velocity is deemed subject to biases from float grounding, and is omitted from any calculations. This screening eliminates 26 out of 555 float displacements.

3. Mid-depth velocities

The 10-day float displacements at 1000 dbar (Fig. 2) report a speed mean and standard deviation of 0.039 (±0.025) m s^{-1} in the Aleutian Basin (excluding groundings). The largest displacements (highest speeds) occur when the floats are describing roughly circular motions (both cyclonic and anticyclonic) with radii sometimes approaching 100 km. The radii are much larger than the local 17-km first baroclinic radius of deformation for the Bering Sea (Chelton et al. 1998). Typical speeds within these eddies are around 0.08 m s^{-1} at 1000 dbar, and the floats take slightly less than 100 days to make a single circuit, although not many stay in an eddy for an entire circuit. Eddies of similar size have been observed in hydrographic data (Kinder et al. 1980) where surface geostrophic velocities in the eddies referenced to 1500 dbar were about 0.08 m s^{-1} less than those measured by surface drifters. This difference is very close to the eddy velocities observed at 1000 dbar by the floats, and both imply a potential eddy expression at the bottom. A study using shipboard ADCP data to reference geostrophic velocities confirms that eddy velocities can reach to the bottom (Cokelet et al., 1996).

The 1000-dbar velocity data are analyzed in 0.5° latitude by 1° longitude bins (roughly

55 km by 55 km at this latitude), to produce a mean field with error estimates (Fig. 3). First float displacements from apparently grounded instruments are excluded. Then velocities are computed from displacements and each velocity is assigned a position that is the average of the last position fix before the float sinks and the first position fix after it rises again. The mean velocity in each bin is computed, and deviations from those means are used to compute a current ellipse (Emery and Thomson 1997). Each velocity results from a 10-day displacement. Integral time scales from velocity autocovariances for the float displacements (not shown) suggest that each velocity measurement is independent, so the current ellipses can be scaled using the number of observations in the bin and Student's t-distribution to obtain a 95% confidence limit for the mean velocity vectors (Fig. 3).

Mean velocities are generally less than 0.05 m s^{-1}, not well-organized, and not significantly different from zero at 95% confidence limits (Fig. 3). With vigorous eddy signatures in much of the Bering Sea, even at 1000-dbar, it is not surprising that the mean there is difficult to determine. However, it is still early in the history of the array, so the means are likely to become better known with time.

The one exception to this lack of pattern is the group of more rapid and coherent northwestward velocities found offshore of the Bering Shelf, the 1000-dbar signature of the Bering Slope Current. This current is visible in the individual float displacements (Fig. 2) and in the general tendency for the mean velocities in the bins closest to the 1000-m isobath to flow northwestward, paralleling the isobaths (Fig. 3). Many of the mean values in these bins are significantly different from zero at 95% confidence limits. Since geostrophic transport estimates of this current frequently assume a level of no motion near this pressure, accurate estimates of the observed along-slope velocity at this pressure are desirable to

improve transport estimates. The Aleutian North Slope Current is not apparent in the float displacements, perhaps because it is centered over the 1000-m isobath and is narrower than the Bering Slope Current (Stabeno and Reed 2003).

More detailed estimates of the along-slope velocity field at 1000-dbar associated with the Bering Slope Current are made. First, the closest range to the 1000-m isobath and the bearing associated with that range is found for the mean position of each float park velocity. Only data within the region containing the current are included (southwest of the Bering Shelf within the Aleutian Basin, Fig. 1). There are 265 velocity estimates (each estimate independent as mentioned above) within the study region, over 7 float-years of data. The bearing for each velocity location is used to rotate the velocity data into along-slope and across-slope components of the flow. The along-slope velocities are then averaged according to range from the 1000-m isobath in 20-km bins, containing between 20 and 34 points in each bin out to 160 km (Fig. 4), and fewer further offshore.

The signature of the Bering Slope Current is evident in the 3 bins closest to the 1000-m isobath, with velocities reaching as high as 0.028 (±0.010) m s^{-1} at 50 km from the coast. Values in the bins 30 and 50 km from the 1000-m isobath (positive values signify flow in a cyclonic sense around the basin) are significantly different from zero within 95% confidence limits, the uncertainties quoted, whereas the bins further offshore have values that are much closer to zero and are not statistically different from zero.

While these flows are not large when compared with surface velocities (Stabeno and Reed 1994), even small flows integrated over the water column can amount to a significant transport. If these 1000-dbar flows are applied as depth-independent between the surface and 1000 dbar and then integrated offshore of 1000-m isobath as a function of range, they amount

to 1.1 (±0.4) Sv by 70 km offshore (Fig. 4). This transport is significant fraction of the previous 5 Sv estimate for the Bering Slope Current above a 1500-dbar level of no motion (Kinder et al. 1975). However, this estimate of the effect of the 1000-dbar velocities on the current transport is a conservative one, because the flow undoubtedly extends below 1000 dbar (Roden 1995, Cokelet et al. 1996), even with geostrophic shear acting to diminish velocities toward the sea floor.

4. Water property distributions

The Bering Sea pycnocline is dominated by salinity stratification, with a stabilizing layer of fresh water overlying saltier water at depth (Fig. 5a, Roden 1995). In contrast, the θ distribution includes a subsurface maximum within the permanent pycnocline (Fig. 5b, near 300 dbar) that originates from inflow of relatively warm Alaska Stream water into the Bering Sea through the passes in the southern island arc (Reed 1995), modified by strong mixing within the passes. Above that maximum is a θ minimum (Fig. 5b, thick line near 200 dbar), evident below the seasonal thermocline in all but the most extreme winter conditions (Fig. 5b, thin line), when the minimum is renewed by surface cooling (Cokelet and Stabeno 1997). These features can be used to infer the circulation patterns (Kinder et al. 1975). The hydrographic data collected between the float park pressure and the surface are exploited here to examine these water property distributions.

The mean potential density of the subsurface θ minimum is $\sigma_\theta = 26.60$ kg m^{-3}. This value is very close to the maximum wintertime mixed layer σ_θ observed by the floats, as would be expected for a feature renewed by wintertime surface cooling. While there is a lot

of scatter in θ on this potential isopycnal, the data show a clear seasonal cycle (Fig. 6). This cycle is described here by annual and semiannual harmonics fit to the data. The isopycnal rapidly cools over the winter season, from a high of 3.4°C in December to a low of 2.7°C in April, just after the mixed layer is coldest, densest, and deepest. It then warms more slowly, over the rest of the year, presumably owing to some combination of mixing acting on the vertical extrema, and advection of warmer Alaska Stream water into the Bering Sea through the southern island arc passes (Stabeno and Reed 2003).

An objective map of θ on σ_θ = 26.60 kg m^{-3}, with the seasonal cycle removed, shows a relatively clear spatial pattern, colder in the center of the basin and warmer near the boundaries (Fig. 7). The warm signature is strongest near its source, consisting of flow through and mixing within the island arc passes. These warm waters appear to be advected eastward along the southern boundary of the Aleutian Basin in the Aleutian North Slope Current and then northwestward along the northeastern boundary of the basin in the Bering Slope Current. The θ field on σ_θ = 26.60 kg m^{-3} is of course subject to cooling by ventilation at the height of winter, but presumably the inflow of warmer waters from the Alaska Stream counterbalances the wintertime heat loss.

From the float deployment period to date, the subsurface θ maximum has tended toward the cold (~ 3.8°C), dense (σ_θ ~ 26.81 kg m^{-3}), and deep (p ~ 314 dbar) end of historical values in the region (Reed 1995). Interannual variability of this maximum is attributed to variability in the inflow from the south, and hydrographic surveys in some years show much warmer water associated with the Aleutian North Slope Current than in others (Reed 1995). The conditions observed by the float array suggest relatively weak inflow of the Alaska Stream water through the passes during the float observation period. The θ values

at the mean σ_θ of the θ maximum (not shown) are relatively uniform temporally. This potential isopycnal is well below the wintertime mixed layer, and there is no significant seasonal cycle in θ on it. The only discernible feature is a slight cooling of 0.05°C over the 19.5-month record. The spatial distribution of this field (also not show) is like an attenuated version of the map on the median potential density of the shallow θ minimum.

For a more detailed examination of the water property distributions associated with the Bering Slope Current, data are again analyzed as a function of range from the 1000-m isobath using data from the same region used for the 1000-dbar float velocity estimates within the current (Fig. 1). The float θ and S data are linearly interpolated to a 10-dbar pressure grid. Mean seasonal cycles (annual and semiannual harmonics) are fit to both water properties using all data within the region on each pressure surface. These seasonal cycles are then removed. The data so modified are then smoothed as a function of range on each pressure surface using a loess filter (Cleveland and Devlin 1988) with a 60-km half power point. This processing averages over along-slope variations and eddies.

The resulting mean salinity section (Fig. 8a) illustrates several features associated with the Bering Slope Current. Of course S increases monotonically downward as expected in the Bering Sea. The isohalines, which largely follow isopycnals (not shown) tilt downward as they approach the continental slope. This tilt is a signature of the along-slope geostrophic shear in this current, with surface-intensified northwestward flow. There is clearly mean geostrophic shear associated with the current that extends all the way to 1000 dbar. Unfortunately, the infrequent sampling below 1000 dbar (every 4th profile extends to a target pressure of 2000 dbar) makes detailed analysis of water property distributions below 1000 dbar a dubious exercise at present. Another prominent feature is the significant freshening of

surface water approaching the continental slope, a signature of the transition between open ocean and shelf waters (Kinder and Coachman 1978).

The mean θ section (Fig. 8b) also reveals patterns typical of the Bering Slope Current. In the Bering Sea, salinity dominates the stratification, so temperature is closer to a passive tracer than in many other regions. The subsurface θ minimum, found near 150 dbar, weakens towards the slope. This weakening is a signature of the Bering Slope Current, and caused by northwestward advection of warm water from the south within the current (Kinder et al. 1975). This pattern is also evident on isopycnal maps (Fig. 7). The more subtle subsurface θ maximum is found between 300 dbar and 400 dbar. It strengthens slightly (although not visibly) towards the slope, as expected given its southern source and the cyclonic circulation. The surface layer (roughly mid-way between summer and winter values, as expected since the seasonal cycle has been removed) has a θ that increases slightly toward the continental slope.

5. Geostrophic flow

In addition to velocity estimates at the park pressure of 1000 dbar, the floats allow application of the geostrophic relation between the park pressure and the surface to obtain circulation information. The floats often take their deepest measurements slightly shallower than 1000 dbar, so geostrophic calculations are made between the sea surface and 990 dbar, relative to 990 dbar. In addition, since these calculations involve vertical integration, only profiles with data from all nominal pressures are used, limiting the data set to 465 profiles.

The transport function Q (Sverdrup et al. 1942, pp. 463) is just the vertical integral of the geopotential anomaly, referenced as desired, between two pressures. This quantity is used

here to analyze the geostrophic transport between the surface and 990 dbar, relative to 990 dbar. Relative volume transports over this pressure range are locally parallel to Q isopleths. Transports between Q isopleths are found by dividing their difference by f, the local Coriolis parameter. If the range of the Coriolis parameter is small, an approximate relative transport stream function can be constructed from Q/f_o, where $f_o = 1.26 \times 10^{-4}\ s^{-1}$ is the Coriolis parameter for the central latitude of the region of interest, 56.5°N for the deep Bering Sea. This approximate transport stream function is biased about 5% low at the southern limit of the deep Bering Sea, and about 5% high at its northern limit, small errors in comparison with other noise sources. Differences of this quantity, and not its absolute value, yield transport estimates, analogous to the relation between dynamic height gradients and geostrophic velocity.

The annual cycle of Q/f_o, (Fig. 9) has its lowest values in April and highest values in September. When estimated over the entire basin the observed seasonal cycle reflects mostly the seasonal temperature variability from the upper ocean. This variability has no direct relation to seasonal transport variations within the basin, since it does not involve a spatial difference in Q/f_o. The seasonal cycle is removed prior to further analysis. Numerical model results suggest there may also be a seasonal cycle in basin current transports (Overland et al. 1994) due to variability in wind forcing (Bond et al. 1994). However, this cycle can not yet be estimated with the float data.

An objective map of Q/f_o, reveals a familiar pattern, with relatively low values in the center of the basin, and higher values around the periphery (Fig. 10). The map is made under the same assumptions that were previously made for mapping the θ-minimum. The higher values along the southern boundary of the Aleutian Basin are the signatures of the eastward

flowing Aleutian North Slope Current. The higher values on the northeastern boundary of the Aleutian Basin are the signatures of the northwestward flowing Bering Slope Current. The significant variability in the values even after the mean seasonal cycle is removed is primarily the signature of mesoscale eddies (Mizobata et al. 2002). The sampling density is not yet sufficient to overcome the effect of this variability as mapped. One might expect a relatively constant transport stream function around the rim of the Aleutian Basin. However, as a result of the influence of eddies, the mapped values at the boundary exceed the central minimum mapped value by between 0.5 Sv and 5 Sv.

Analysis of Q/f_o, as a function of range from the 1000-m isobath within the Bering Slope Current region allows an estimate of the current transport between the surface and 990 dbar relative to 990 dbar using 232 data points (Fig. 11). The transport depends on the difference of a value representative of Q/f_o at the 1000-m isobath and some (hopefully constant) offshore value. Fitting an exponential function to these data versus range is one way to estimate the transport and lateral scale of the current. This model gives a current transport of 2.9 (±0.6) Sv and a lateral scale of 80 (±70) km, where the 95% uncertainties have been determined using a delete-one jackknife (Efron 1982).

While the continental slope is steep in this region, there is a small cross-sectional area between the 1000-m isobath and the shelf break. This region is not sampled by the floats unless they run aground, which fortunately is an infrequent occurrence. The Bering Slope Current does extend inshore of the 1000-m isobath (Kinder et al. 1975). However the small cross-sectional area in which it has to flow limits the transport contribution of this portion of the current (which can not be estimated here) to the overall transport in the current.

6. Discussion

One could use the direct velocity estimates at the float park pressure of 1000 dbar to construct a level of known motion at 1000 dbar (Davis 1998), rather than relying on the assumption of a level of no motion at 990 dbar. However, given the rather noisy and uncertain nature of the estimates outside of the Bering Slope Current (Fig. 6), this exercise can not yet be done throughout the basin. The transport in the upper 1000 dbar within the current resulting from the direct velocity estimates at 1000 dbar is 1.1 (±0.4) Sv (Fig. 4) between the 1000-m isobath and 70 km offshore. This value can be combined with the geostrophic transport estimate above made between the surface and 990 dbar, relative to 990 dbar (Fig. 10) to get an absolute estimate of the current transport, 4.0 (±0.8) Sv above 1000 dbar and offshore of the 1000-m isobath.

Significant along-shore velocities within the Bering Slope Current at the park pressure (Fig. 4) suggest the current extends below 1000 dbar and the transport estimate made here from the surface to 1000 dbar is incomplete. There is clearly vertical geostrophic shear in the current at 1000 dbar (Fig. 4a) which extends below 1000 dbar, presumably slowly diminishing with increasing pressure (Roden 1995, Cokelet et al. 1996). Analyzing Q/f_o between 990 dbar and various deeper pressures (between 1100 - 1800 dbar) relative to 990 dbar (this time without subtraction of a seasonal cycle because none was apparent in Q/f_o at these pressures) shows that the total current transport is largest when integrated between the surface and 1600 dbar. An exponential model results in a transport of -0.4 (±0.2) Sv between 990 and 1600 dbar relative to 990 dbar offshore of the 1000-m isobath and a lateral scale of 70 (±80) km. The relative transport value is negative because the reference level is 990 dbar,

which we know from the direct velocity estimates is too shallow. Summing the direct velocities at the park pressure applied depth independently over 1600 dbar with the geostrophic transports between 0 and 1600 dbar relative to the park pressure gives a net current transport estimate of 4.2 (±1.1) Sv. The large correlation between Q/f_o above and below 990 dbar has been taken into account in propagating errors. This mean estimate is only slightly larger than that above 1000 dbar, suggesting that most of the current is found above 1000 dbar.

Acknowledgments. This work was funded by the NOAA National Marine Fisheries Service Steller Sea Lion Coordinated Research Program and the NOAA Office of Oceanic and Atmospheric Research. It work would not have been possible without the very able assistance of Dana Swift and Dale Ripley in float preparation, Donald Denbo and Kristene McTaggart in float data management, and many helpful colleagues in float deployment.

REFERENCES

Bond, N. A., J. E. Overland, and P. Turet, 1994: Spatial and temporal characteristics of the wind forcing of the Bering Sea, *J. Climate*, **7**, 1119-1130.

Chelton, D. B., R. A. deSzoeke, M. G. Schlax, K. El Naggar, and N. Siwertz, 1998: Geographical variability of the first-baroclinic Rossby radius of deformation. *J. Phys. Oceanogr.*, **28**, 433-460.

Cleveland, W. S., and S. J. Devlin, 1988: Locally weighted regression: An approach to regression analysis by local fitting. *J. Am. Stat. Assoc.*, **83**, 596-610.

Cokelet, E. D., M. L. Schall, and D. M. Dougherty, 1996: ADCP-referenced geostrophic circulation in the Bering Sea basin, *J. Phys. Oceanogr.*, **26**, 1113-1128.

Cokelet, E. D., and P. J. Stabeno, 1997: Mooring observations of the thermal structure, salinity, and currents in the SE Bering Sea basin, *J. Geophys. Res.*, **102**, 22947-22964.

Davis, R. E., 1998: Preliminary results from directly measuring middepth circulation in the tropical and South Pacific, *J. Geophys. Res.*, **103**, 24619-24639.

Efron, B., 1982: *The Jackknife, the Bootstrap, and Other Resampling Plans*. CBMS-NSF Regional Conference Series in Applied Mathematics, 38, SIAM, Philadelphia, 92 pp.

Emery, W. J., and R. E. Thompson, 1997: *Data Analysis Methods in Physical Oceanography*, Elsevier Science Inc., New York, NY, USA, pp. 634.

Kinder, T. H., and L. K. Coachman, 1978: The front overlaying the continental slope in the eastern Bering Sea, *J. Geophys. Res.*, **83**, 4551-4559.

Kinder, T. H., L. K. Coachman, and J. A. Galt, 1975: The Bering Slope Current System, *J. Phys. Oceanogr.*, **5**, 231-244.

Kinder, T. H., J. D. Schumacher, and D. V. Hansen, 1980: Observation of a baroclinic eddy: an example of mesoscale variability in the Bering Sea, *J. Phys. Oceanogr.*, **10**, 1228-1245.

Mizobata, K., S. I. Saitoh, A. Shiomoto, T. Miyamura, N. Shiga, K. Imai, M. Toratani, Y. Kajiwara, and K. Sasoaka, 2002: Bering Sea cyclonic and anticyclonic eddies observed during summer 2000 and 2001, *Prog. Oceanogr.*, **55**, 65-75.

Okkonen, S. R., 2001. Altimeter observations of the Bering Slope Current eddy field, *J. Geophys. Res.*, **106**, 2465-2476.

Overland, J. E., M. C. Spillane, H. E. Hurlburt, and A. J. Wallcraft, 1994: A numerical study

of the Bering Sea Basin and exchange with the North Pacific Ocean, *J. Phys. Oceaongr.*, **24**, 736-758.

Reed, R. K., 1995: On the variable subsurface environment of fish stocks in the Bering Sea, *Fish. Oceaongr.*, **4**, 317-323.

Reed, R. K., 1995: On geostrophic reference levels in the Bering Sea, *J. Oceanogr.*, **51**, 489-498.

Reed, R. K., and P. J. Stabeno, 1994: Flow along and across the Aleutian Ridge, *J. Mar. Res.*, **52**, 639-648.

Roden, G. I., 1994: Aleutian Basin of the Bering Sea: Thermohaline, oxygen, nutrient and current structure in July 1993, *J. Geophys. Res.*, **100**, 13539-13554.

Schumacher, J. D., and R. K. Reed, 1992: Characteristics of currents over the continental slope of the eastern Bering Sea, *J. Geophys. Res.*, **97**, 9423-9433.

Schumacher, J. D., and P. J. Stabeno, 1994: Ubiquitous eddies of the eastern Bering Sea and their coincidence with concentrations of larval pollack, *Fish. Oceaongr.*, **3**, 182-190.

Smith, W. H. F., and D. T. Sandwell, 1997: Global sea floor topography from satellite altimetry and ship depth soundings, *Science*, **277**, 1956-1962.

Stabeno, P. J., and R. K. Reed, 1992: A major circulation anomaly in the western Bering Sea, *Geophys. Res. Lett.*, **19**, 1671-1674.

Stabeno, P. J., and R. K. Reed, 1994: Circulation in the Bering Sea Basin observed by satellite-tracked drifters: 1986-1993, *J. Phys. Oceanogr.*, **24**, 848-854.

Stabeno, P. J., and R. K. Reed, 2003: Observations of the Aleutian North Slope Current, Bering Sea, 1996-2000, *Prog. Oceanogr.*, in preparation.

Stabeno, P. J., J. D. Schumacher, and K. Ohtani, 1999: The physical oceanography of the

Bering Sea. T. R. Louglin and K. Ohtani, Eds., *Dynamics of the Bering Sea: A Summary of Physical, Chemical, and Biological Characteristics, and a Synopsis of Research on the Bering Sea*, Sydney, British Columbia and Fairbanks, Alaska: North Pacific Marine Science Organization (PICES) and University of Alaska Sea Grant, AK-SG-99-03, 1-28.

Sverdup, H. U., M. W. Johnson, and R. H. Fleming, 1942: *The Oceans: Their Physics, Chemistry, and General Biology*, Prentice-Hall Inc., Englewood Cliffs, NJ, USA, pp. 1087.

Verkhunov, A. V., and Y. Y. Tkachenko, 1992: Recent observations of variability in the western Bering Sea current system, *J. Geophys. Res.*, **97**, 14369-14376.

Wong, A. P. S, G. C. Johnson, and W. B. Owens, 2003: Delayed-mode calibration of autonomous CTD profiling float salinity data by theta-S climatology, *J. Atmos. Oceanic Technol.*, in press.

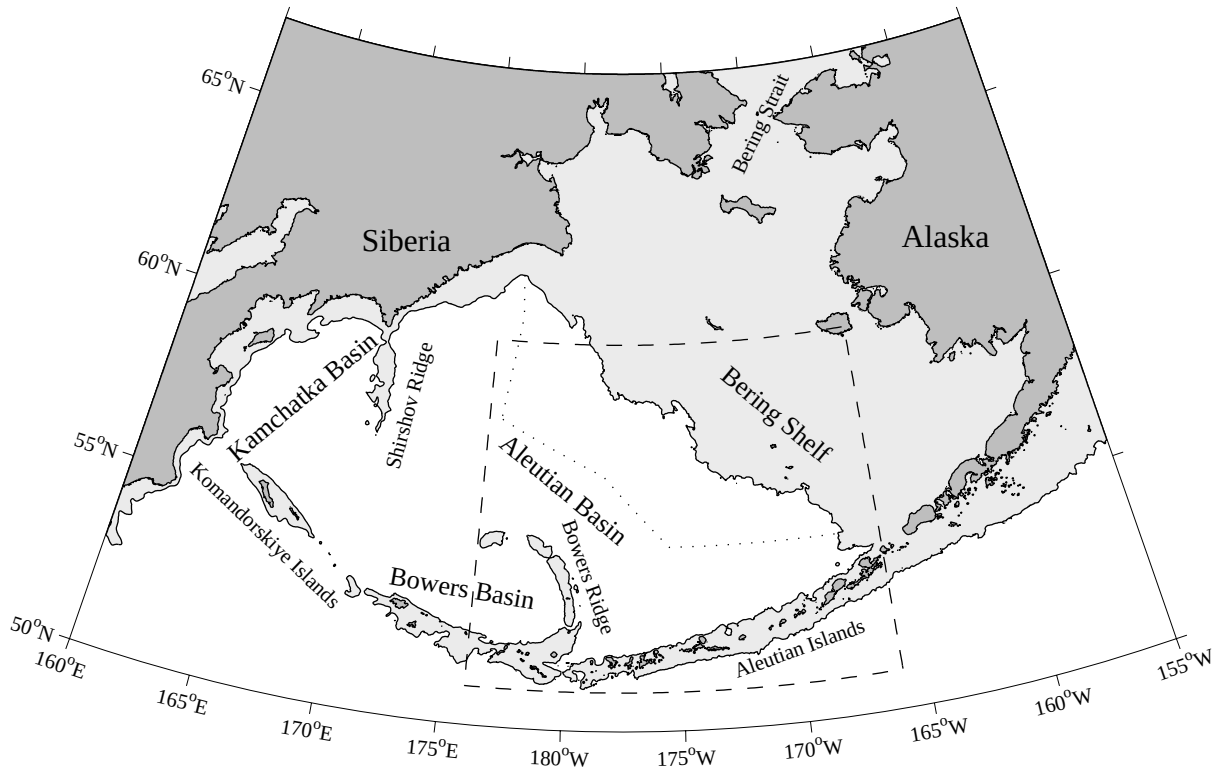

Fig. 1. Bering Sea region with place names. Depths shallower than 1000 m are lightly shaded and land is heavily shaded using version 8.2 bathymetry of Smith and Sandwell (1997). The dashed line indicates the float array region, and the Bering Slope Current study region is located northeast of the dotted line.

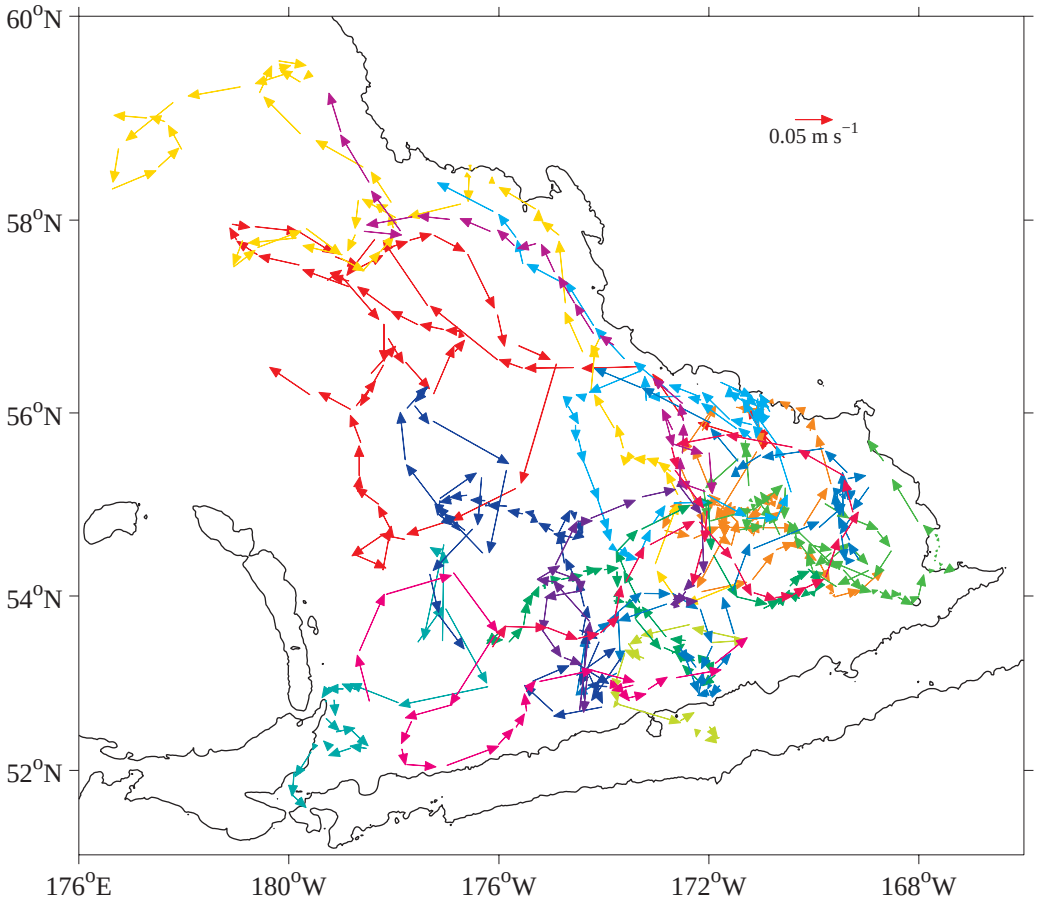

Fig. 2. All 10-day displacements at 1000 dbar (including grounded values) from the CTD profiling floats in the Bering Sea. A velocity scale is over the Bering Shelf. The 1000 m isobath (thin line) is displayed for reference.

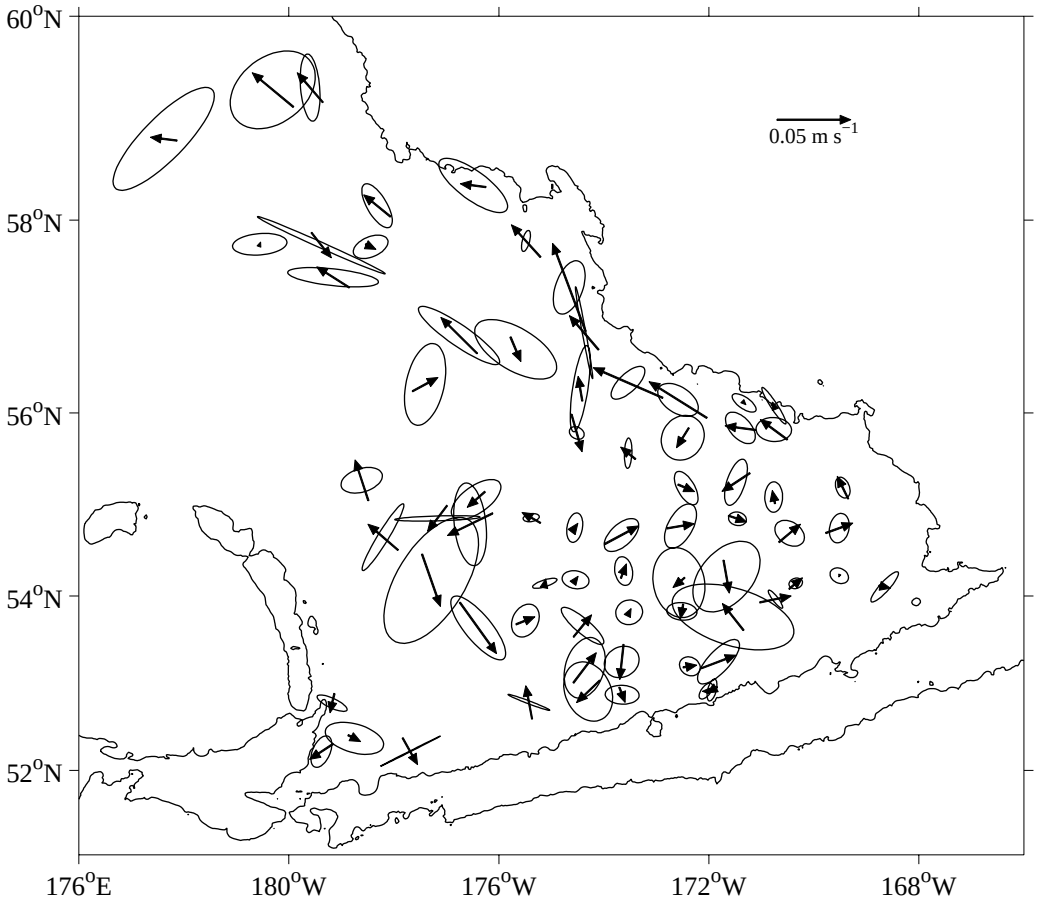

Fig. 3. Mean velocities and error ellipses at 1000 dbar constructed from analysis of individual float displacements (excluding grounded values) in 0.5 latitude by 1 longitude bins. Results from bins containing at least three measurements are shown, using 88% of the individual displacements. Arrows are centered on the mean position of the velocity measurements within the bins. Current error ellipses are scaled so that if the mean vector reaches outside the error ellipse, it is significant at 95% confidence limits. Details follow Fig. 2, except for a change in velocity scale.

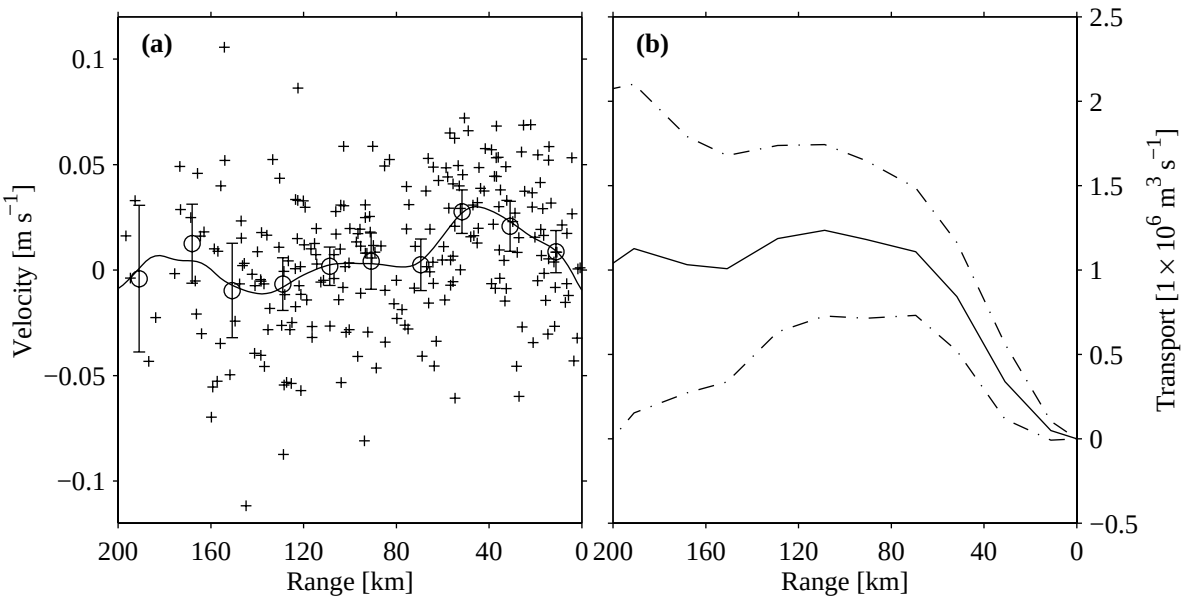

Fig. 4. (a) Along-slope velocities within the Bering Slope Current as a function of range from the 1000-m isobath with raw values (+'s), averages in 20-km bins (o's with error bars showing 95% confidence intervals), and a smooth curve drawn using a loess filter with a 40-km half-power point (solid line). (b) Cumulative transport resulting from application of the binned 1000-dbar velocities and their uncertainties over 0-1000 dbar integrated as a function of range from the 1000-m isobath (solid lines) with 95% confidence intervals (dot-dashed lines). Range is plotted in reverse to associate northeast with the right hand side.

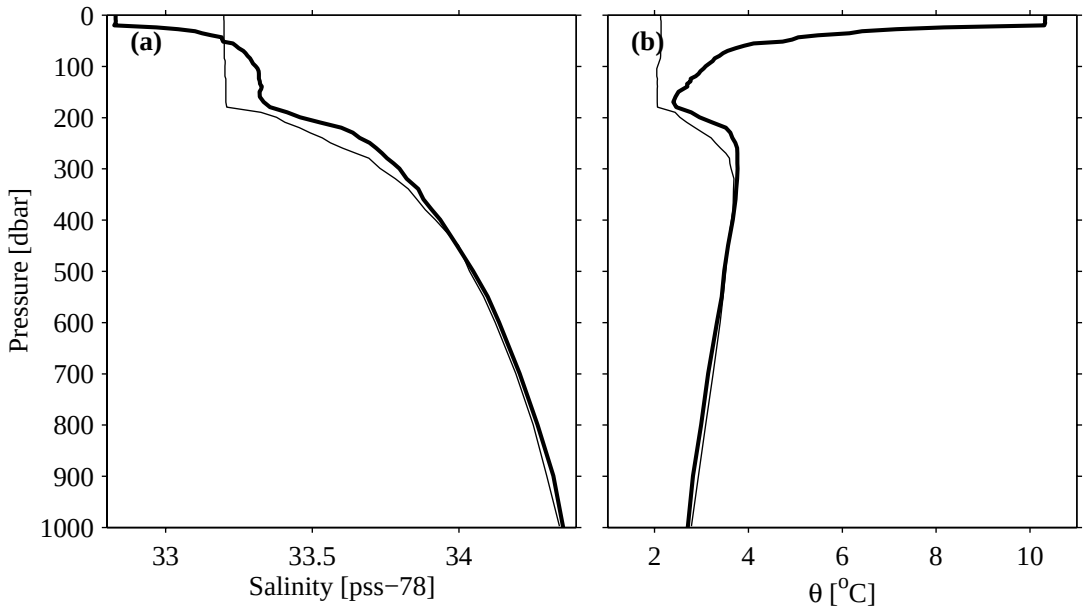

Fig. 5. Vertical profiles of (a) salinity and (b) potential temperature (θ) plotted against pressure. A summer profile taken at 56.56° N, 176.00°W on 21 August 2001 (thick lines) is contrasted with a winter profile taken at 56.77°N, 176.65°W on 16 January 2002 (thin lines).

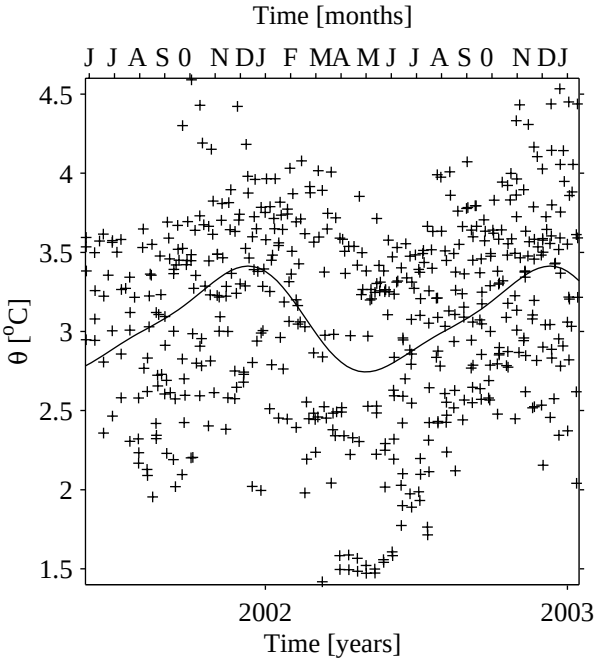

Fig. 6. Potential temperature (θ) on the mean potential density of the shallow θ minimum, σ_θ = 26.60 kg m^{-3}, from the Bering Sea float data (dots) plotted against time. A mean seasonal cycle is described by annual and semiannual harmonics fit to the data (solid line).

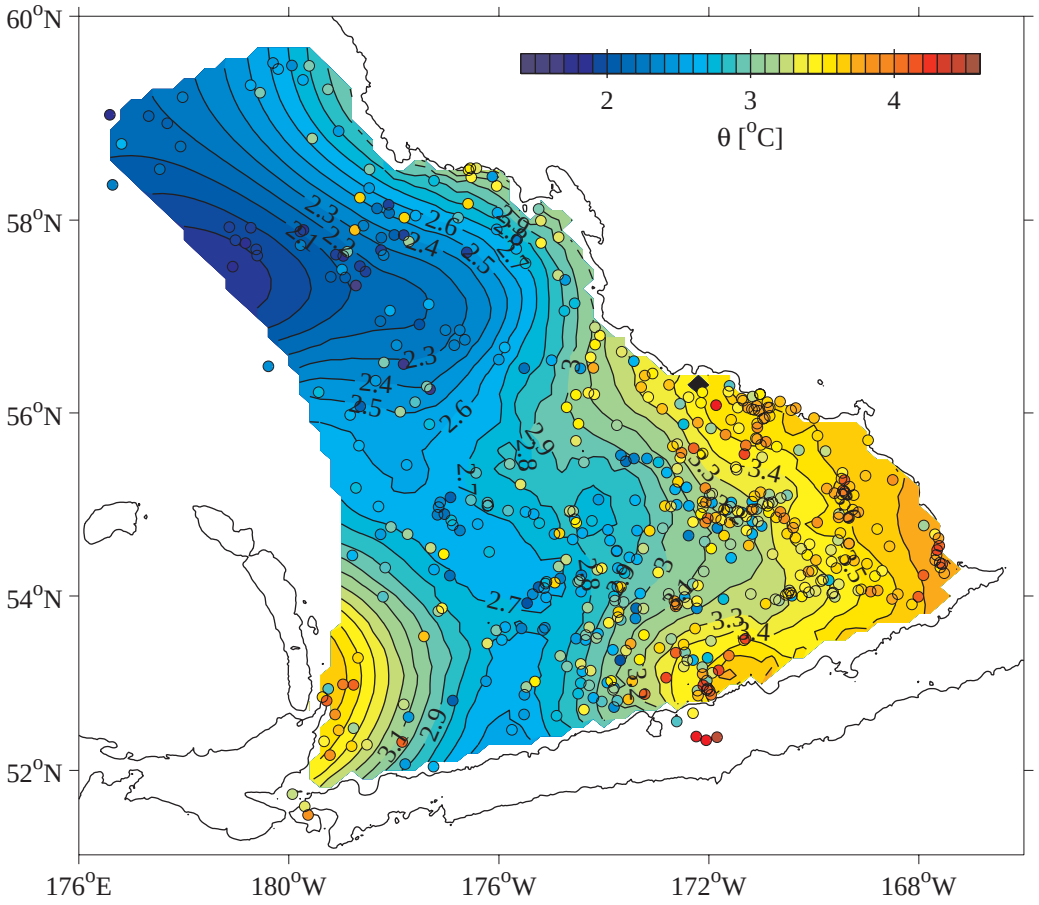

Fig. 7. Objective map of potential temperature (θ) on the mean potential density of the shallow θ minimum, σ_θ = 26.60 kg m^{-3}. The mean seasonal cycle (Fig. 6) is removed from the data prior to mapping. The map assumes a Gaussian covariance incorporating correlation scales of 4° longitude, 2° latitude, and 2 × 10^{-7} m^{-1} s^{-1} in potential vorticity (the Coriolis parameter f over water depth h) and a noise-to-signal energy of 0.0625. Contours (at 0.1°C intervals) stop where mapping errors exceed the assumed noise-to-signal energy. Data values (dots) are shaded with the same color scale used for the contours.

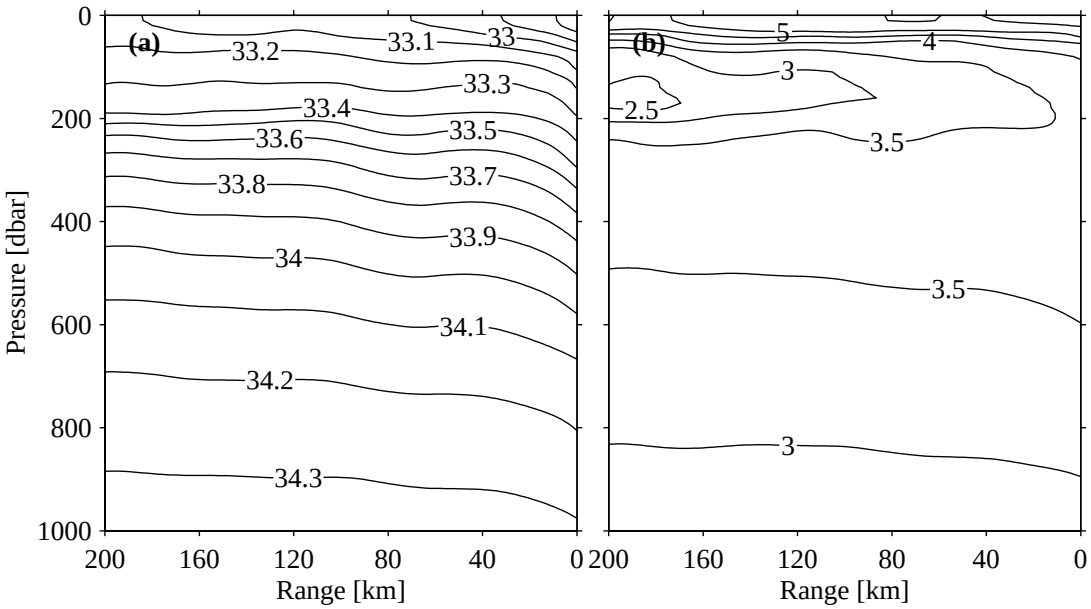

Fig. 8. Mean vertical sections of (a) salinity (S) contoured at 0.1 intervals and (b) potential temperature (θ) contoured at 0.5°C intervals as a function of pressure and range from the 1000-m isobath in the region of the Bering Slope Current.

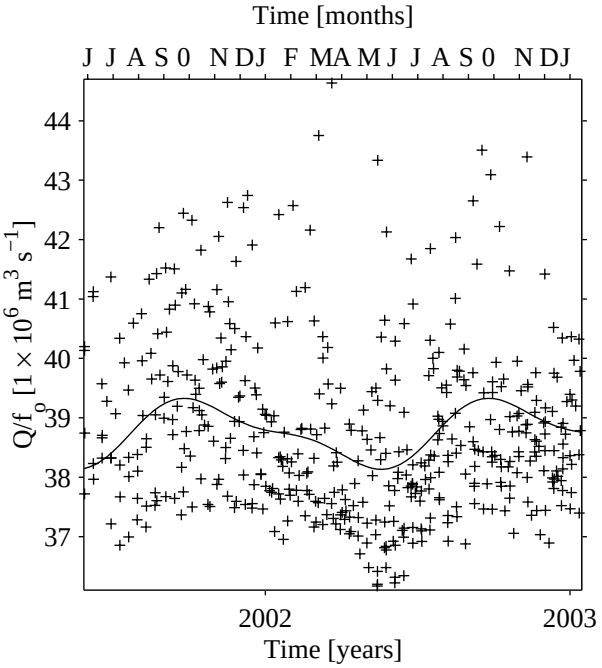

Fig. 9. Approximate transport stream function Q/f_o (1×10^6 m^3 s^{-1}) between the surface and 990 dbar, relative to 990 dbar, from the Bering Sea float data (+'s) plotted against time. A mean seasonal cycle is described by annual and semiannual harmonics fit to the data (solid line).

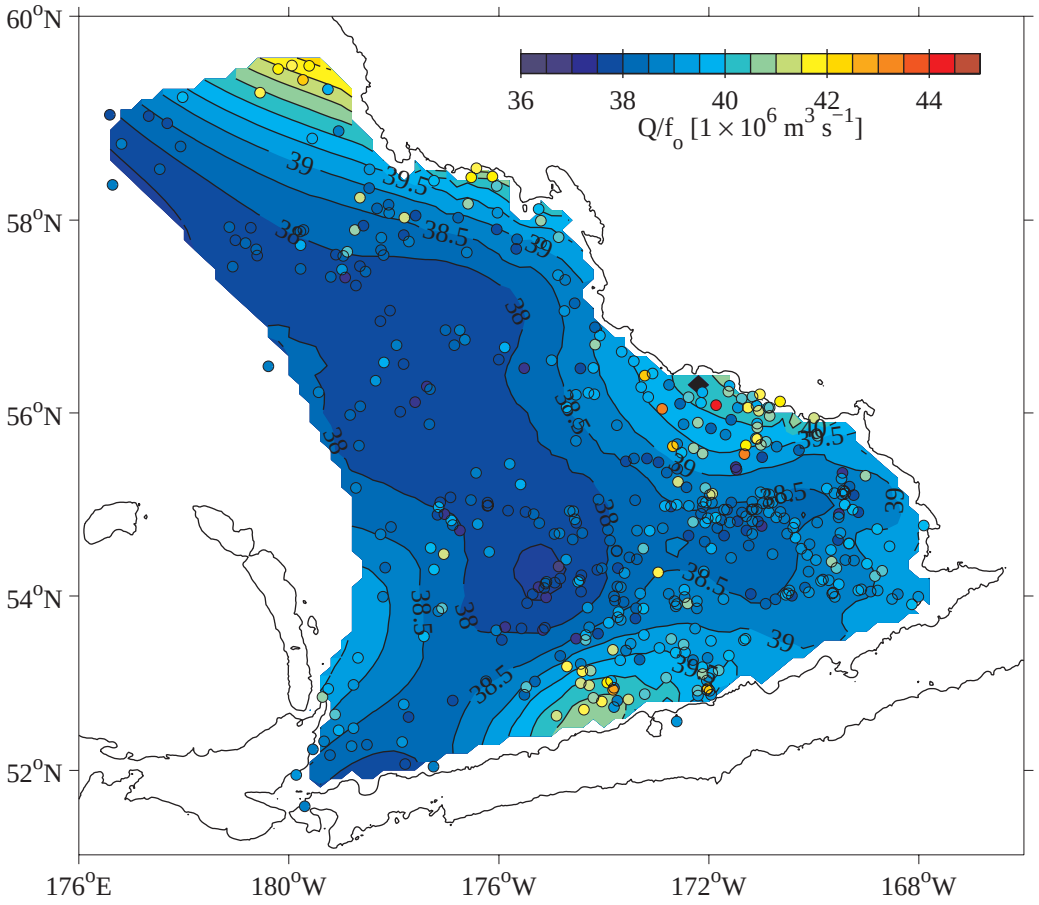

Fig. 10. Approximate transport stream function Q/f_o between the surface and 990 dbar, relative to 990 dbar, from the Bering Sea float data contoured at 0.5 $\times 10^6$ m^3 s^{-1} intervals. Details follow Fig. 7.

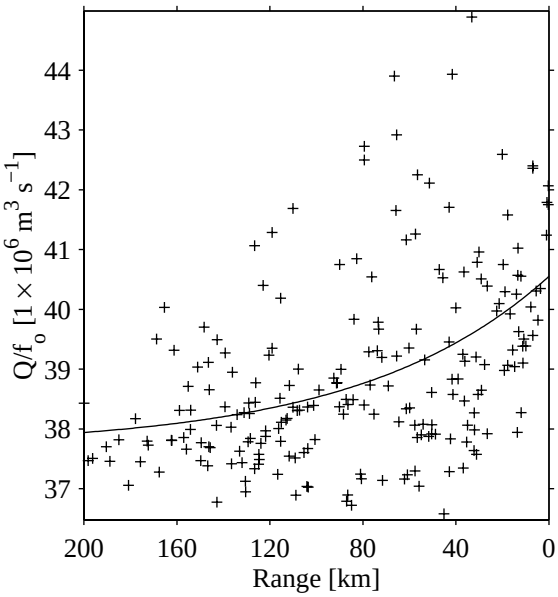

Fig. 11. Approximate transport stream function Q/f_o between the surface and 990 dbar, relative to 990 dbar within the Bering Slope Current study region plotted as a function of range from the 1000-m isobath. An exponential fit to Q/f_o versus range (solid line) allows transport and lateral scale estimates for the current.